Statistical power and measurement bias in multi-centric resting-state fMRI connectivity

Christian Dansereau[a,b], Celine Risterucci[c], Emilio Merlo Pich[c], Douglas Arnold[d], Pierre Bellec[a,b,*]

[a] *Centre de Recherche de l'Institut Universitaire de Gériatrie de Montréal, Montréal, CA*
[b] *Département d'Informatique et de recherche opérationnelle, Université de Montréal, Montréal,CA*
[c] *F. Hoffmann-La Roche Ldt., Basel, Switzerland*
[d] *NeuroRx, Montreal, Quebec, Canada*

Abstract

Keywords: multisite, multiprotocol, bias, statistical power, sample size, resting-state, fMRI, connectivity

Highlights

- etc

1. Introduction

Resting-state (RS) connectivity in fMRI is a promising biomarker for a variety of neurological diseases. Although, there is increasing concern about the reliability and reproducibility of scientific research and findings. One major source of concern within neuroscience is the low statistical power of many published studies, given that this increases the proportion of published findings that are false and can create unwanted biases or difficulty to detect small and consistent effect (differences) between groups. These worries have increased pressure to amass larger samples, but in many cases this is not feasible due to recruitment constraints (for example, when the number of subjects with a particular disorder in any geographical area is limited) or financial limitations. A solution to that problem is to increase the number of subject by pooling small RS cohorts acquired on the same scanner or on different scanners, this approach is referred to has multisite acquisition. Multi-site study are more and more common in fMRI and a lot of initiative have started to emerge to provide public data acquired at multiple sites. Has reported by Cheng et al. (2015) there is an urgent need to use methods that will allow large-scale pooling of data to both reduce

*Corresponding author
Email address: pierre.bellec@criugm.qc.ca (Pierre Bellec)

the impact of heterogeneity between studies and allow the study of stratified subgroups. Nevertheless, multi-centric studies come with there share of advantages and disadvantages. The main advantages are the rapid recruitment of large sample-size across multiple sites and potentially distant geographically. This parallel recruitment provide better generalization due to more diversity in the scanners used although result in potential new sources of variance. This bias in measurement originating from the various acquisitions sites may decrease the benefit of a large sample-size due to the added variability in the data. We are therefore taking advantage of a public fMRI resource that incorporate these kind of variabilities to address this question and several others.

Mutisite. In most experiments conducted in neuroimaging, the main factors that influence power are: (1) the size of the effect, determined by the difference of the mean connectivity of one group versus a control group and the variability of this difference across subjects and groups; and (2) the sample size, i.e. the number of subjects in the study (Desmond and Glover, 2002). This last factor is usually the only one controlled by the investigator, hence why an increasing number of researchers share data. Multisite studies can be classified in two categories, the first one is independent studies that we would like to pool together even though the acquisition protocol are heterogeneous like the 1000 functional connectome project. The second category is the standardised studies across multiple sites, were a strict protocol is in place to harmonize the sites and an effort to homogenize the scanner parameters et acquisition protocols as been done like the ADNI dataset. Various reasons can justify multisite analysis, in research it is very difficult to obtain a grant large enough to scan a cohort larger than 80 subjects, therefore researcher and consortium initiatives have started to pool their resources together to make initiative composed of publicly available large cohorts of subjects like the 1000 functional connectome (Biswal et al., 2010), ADNI (Mueller et al., 2005), among others. In clinical trial the justification for multicentric acquisition is more of a logistical one then a financial reason; they need to recruit a large amount of subject in a short period of time. In order to achieve this goal they mandate the recruitment to multiple clinical centers across the globe which accelerate the evaluation time of a drug. Although these centers may be similar by their scanner protocols, scanners will have difference in their software version, specific add-on to the scanners, and, most importantly, vendors (even field strength may differ in some cases). Unfortunately between studies, MR acquisition methodologies are among the most commonly cited sources of measurement variation (Friedman et al., 2006). This is why it is important to assess if multi-site resting-state connectivity analysis are feasible (we can combine the data from multiple sources while introducing a reasonable amount of variance which is still acceptable to detect effects in the data) and what corrective measure on the data should be applied to reduce the bias introduced by multisite analysis.

Sources of variance across sites. Beyond small sample sizes resulting in low statistical power (Kelly et al., 2012) and inconsistency in the results, there are

other methodological differences that may compromise the comparison of results across independent studies. For example, the criteria for recruiting subjects may differ among studies. Different study samples may also reflect different socio-cultural characteristics of recruiting sites, e.g., ethnicity, language, diet, socioeconomic status. The fMRI measurements themselves can also be affected by differences in details of the image acquisition such as scanner make and model (Friedman et al., 2006), sequence parameters such as repetition time, flip angle, or acquisition volume (Friedman and Glover, 2006), experimental design such as eyes-open/eyes-closed (Yan et al., 2009) or experiment duration (Van Dijk et al., 2010), and scanning environment such as sound attenuation measures (Elliott et al., 1999), room temperature (Vanhoutte et al., 2006), or head-motion restraint techniques (Edward et al., 2000). Knowing that there is several sources of variance, the question is how much do they affect our analysis and does the trade-off of pooling datasets in exchange for increase variance and sample size worth it. Fortunately some resources exist that allow us to evaluate this question empirically.

Evaluation dataset. In 2009, the publicly released 1000 Functional Connectomes Project (FCP) and International Neuroimaging Data-sharing Initiative (INDI) provided a glimpse of the variability in imaging methodologies employed by the neuroimaging field. The dataset includes rs-fMRI samples independently collected at imaging sites around the world. A noteworthy aspect of this dataset is the variation in almost every parameter of the imaging acquisition methodologies, while the majority of subject-related variables are not reported (due in most cases, to the fact that they were not thoroughly recorded). Despite justifiable scepticism, feasibility analyses demonstrated that meaningful explorations of the aggregate dataset, composed of 24 imaging sites for a grand total of 1093 subjects, could be performed (Biswal et al., 2010). Although no explicit correction for multi-site variability was used, they only use global signal correction (GSC) to normalize subjects which may introduce anti-correlation in the data (Fox et al., 2009; Murphy et al., 2009; Saad et al., 2012; Carbonell et al., 2014; Power et al., 2014). After accounting for site-related differences, the analysis showed brain-behaviour relationships with phenotypic variables such as age, gender, and diagnostic label, and confirmed a variety of prior hypotheses (Biswal et al., 2010; Fair et al., 2012; Tomasi and Volkow, 2010; Zuo et al., 2012). While encouraging, many uncontrolled and unknown factors in the 1000 FCP remain a source of concern, as they spread beyond simple site effects and can limit the datasets utility as highlighted by Yan et al. (2013a). An other compelling proof of multi-site bias is the study reported by Nielsen et al. (2013) where they did an analysis on a single site dataset and a multi-site dataset of subject with autism and concluded that the multi-site autism study classification accuracy significantly outperformed chance but was much lower for multi-site prediction than for previous single site results (Nielsen et al., 2013). We therefore need to keep in mind that the site effect must be taken in account in the analysis or we may reduce our detection power.

Site	Magnet	Scaner brand	Channels	N	N final	Sex	Age	TR	# Slices	# Frames
Baltimore, USA	3T	N/A	N/A	23	21	8M/15F	20-40	2.5	47	123
Berlin, Germany	3T	Siemens Tim Trio	12	26	26	13M/13F	23-44	2.3	34	195
Cambridge, USA	3T	Siemens Tim Trio	12	198	195	75M/123F	18-30	3	47	119
Newark, USA	3T	N/A	N/A	19	17	9M/10F	21-39	2	32	135
NewYork_b, USA	3T	Siemens	N/A	20	18	8M/12F	18-46	2	33	175
Oxford, UK	3T	Siemens Tim Trio	12	22	20	12M/10F	20-35	2	34	175
Queensland, Australia	4T	Bruker	1	19	17	11M/8F	20-34	2.1	36	190
SaintLouis, USA	3T	Siemens Tim Trio	12	31	31	14M/17F	21-29	2.5	32	127

Table 1: Site selected from the 1000 functional connectome dataset.

Specific objectives. The main potential issue with that approach is the lack of consistency in the multisite RS connectivity acquisitions that may obscure clinically relevant information. Therefore the aims of the study were to: (1) characterize the amplitude of the intra-site and inter-site connectivity bias, i.e. the systematic differences in rs-fMRI connectivity across different acquisition sites; (2) Quantify the impact of the inter-site variance on the detection power of a rs-fMRI effect. More specifically how sample size, group balancing and interaction of site-pathology in multi-centric topology impact sensitivity.

2. Method

2.1. Data samples

Participants. The paper studies 345 cognitively normal young adults (CNY) from the 1000 functional connectome project[1] (150 males, age range = 18-46 yrs) as a reference dataset. One of the particularity of this dataset is the presence of one large site of ~ 200 subjects and 7 small sites of ~ 20 subjects per site. We are therefore able to simulate realistic scenarios where we model the variability of a real monosite and the variability introduce by combining small sites into a large sample of the same total sample size, see Table 1 for more details on each site. The experimental protocols for all datasets were approved by there respective ethic boards.

Acquisition. We need to discuss how to present this data (I don't have the details for each site...)

2.2. Preprocessing

The datasets were analysed using the NeuroImaging Analysis Kit (NIAK[2]) version 0.12.14, under CentOS version 6.3 with Octave[3] version 3.8.1 and the Minc toolkit[4] version 0.3.18. Analyses were executed in parallel on the "Mammouth" supercomputer[5], using the pipeline system for Octave and Matlab (Bellec et al., 2010a), version 1.0.2. Brain map visualizations were created using

[1] `http://fcon_1000.projects.nitrc.org/`

[2] `http://www.nitrc.org/projects/niak/`

[3] `http://gnu.octave.org`

[4] `http://www.bic.mni.mcgill.ca/ServicesSoftware/ServicesSoftwareMincToolKit`

[5] `http://www.calculquebec.ca/index.php/en/resources/compute-servers/mammouth-parallele-ii`

MRICron software Rorden et al. (2007). Each fMRI dataset was corrected of inter-slice difference in acquisition time and the parameters of a rigid-body motion was estimated for each time frame. Rigid-body motion was estimated within as well as between runs, using the median volume of the first run as a target. The median volume of one selected fMRI run for each subject was coregistered with a T1 individual scan using Minctracc (Collins et al., 1998), which was itself non-linearly transformed to the Montreal Neurological Institute (MNI) template (Fonov et al., 2011) using the CIVET pipeline (Zijdenbos et al., 2002). The MNI symmetric template was generated from the ICBM152 sample of 152 young adults, after 40 iterations of non-linear coregistration. The rigid-body transform, fMRI-to-T1 transform and T1-to-stereotaxic transform were all combined, and the functional volumes were resampled in the MNI space at a 3 mm isotropic resolution. A censoring method described in (Power et al., 2012) called "scrubbing" was used to remove the volumes with excessive motion using a cut-off value of $FD \geq 0.5$. A minimum number of 50 unscrubbed volumes per run, corresponding to ~ 125 s of acquisition for a TR of 2.5 seconds, was then required for further analysis. The following nuisance parameters were regressed out from the time series at each voxel: slow time drifts (basis of discrete cosines with a 0.01 Hz high-pass cut-off), average signals in conservative masks of the white matter and the lateral ventricles as well as the first principal components (95% energy) of the six rigid-body motion parameters and their squares (Lund et al., 2006),(Giove et al., 2009). The fMRI volumes were finally spatially smoothed with a 6 mm isotropic Gaussian blurring kernel.

2.3. Functional networks

Functional parcellation. Regions are routinely defined using an anatomical parcellation (He et al., 2009), such as the AAL template (Tzourio-Mazoyer et al., 2002). Anatomical parcels may however not well match the brain functional organization. In this work, we used functional brain parcellations, aimed at defining groups of brain regions with homogeneous time series. A number of algorithms have been proposed with additional spatial constraints, to ensure that the resulting parcels are spatially connected (Lu et al., 2003; Thirion et al., 2006; **?**). We can achieve this aim and reduce the computational burden of the analysis using a region-growing algorithm Bellec (2006), resulting in more homogeneous regions composed of temporally similar and contiguous voxels. The spatial dimension was selected arbitrarily by setting the size where the growing process stopped (a threshold of 1000 mm3 resulted into R=957 regions) from a reference dataset of healthy adults from the 1000 functional connectome project (Cambridge cohort (Biswal et al., 2010), parcellation available here 14b). The regions were built to maximize the homogeneity of the time series within the region, i.e. the average correlation between the time series associated with any pair of voxels of the region. The region growing was applied on the time series concatenated across all subjects (after correction to zero mean and unit variance), such that the homogeneity was maximized on average for all subjects, and the small homogeneous regions are identical for all subjects. Because of the temporal concatenation of time series, we had to limit the memory demand,

and the region-growing was thus applied independently in each of the 116 areas of the AAL template (Tzourio-Mazoyer et al., 2002). See Bellec (2006) for more details regarding the implementation of the region-growing algorithm. Overall, this process reduced the dataset of each subject into a (T x R) data array, where T is the number of time samples and R is the number of regions.

Functional network decomposition. From a pure functional viewpoint, the spatial constraint seems somewhat arbitrary, as functional units in the brain at low resolution encompass distributed networks of brain regions with homotopic regions often being part of a single parcel (De Luca et al., 2006; Damoiseaux et al., 2006). Some works have thus used distributed parcels as the spatial units to measure functional brain connectivity, e.g. (Jafri et al., 2007; Marrelec et al., 2008). We relied on a recent method called Bootstrap Analysis of Stable Clusters (BASC), which can identify consistent functional networks for a group of subjects (Biswal et al., 2010). using a hierarchical cluster with Wards criterion both at the individual and the group levels. The functional networks can be generated at any arbitrary scale (within the range of the fMRI resolution), and we considered only networks generated at the group level, which were non-overlapping and not necessarily spatially contiguous. In the present work we generated a BASC decomposition in 100 networks.

TODO: cite the NATURE paper of Pierre Orban for parcelation and connections selection.

Functional connectome. Using a brain partition of R networks obtain from BASC procedure described in Bellec et al. (2010b), and taking each pair of distinct networks i and j, the between-network connectivity $y_{i,j}$ is measured by the Fisher transform of the Pearson's correlation between the average time series of the network. The within-network connectivity $y_{i,i}$ is the Fisher transform of the average correlation between time series of every pair of distinct voxels inside network i. The connectome $\mathbf{Y} = (y_{i,j})_{i,j=1}^{R}$ is thus a $R \times R$ matrix. Each column j (or row, as the matrix is symmetric) codes for the connectivity between network j and all other brain networks (full brain functional connectivity map). For a scale with R parcels, there are exactly $L = R(R+1)/2$ distinct elements in an individual connectome $\mathbf{Y}$.

2.4. Simulations

In order to simulate various scenarios within the context of a multi-site setting, a cohort of subjects acquired at a single-site was selected to act as our reference dataset and for the multi-site configuration a cohort from a collection of small sites, roughly totalling the same sample size as the reference dataset, was used. The simulation was based on a scenario with 8 sites for a total of 345 subjects, and no homogenization of acquisition protocol whatsoever. The multi-site (with correction) is based on 150 subjects from 7 sites and the monosite is based on one site of 195 subjects.

Data generation process. The following data generation model was used to test our hypothesis and estimate how the connectivity bias affect our ability to detect effects at the group level. A sub-sampling procedure was performed on the datasets (monosite and multisite) previously described to obtain multiple samples ($B = 10^3$ random samples). For each of the sample a Monte-Carlo simulation was implemented to evaluate the power of a resting-state multi-site study. For each site and each sample, a ratio W of subjects were randomly assigned to a 'treatment' group, this ratio W is referred to as the allocation ratio of participants. For the subjects in this group, a value was added to achieve a given relative effect size (Cohen's d, i.e. the mean of the two groups divided by the standard deviation of all sites, see Equation 2 for more details).

Effect size (cohen's d). The normalized Cohen's d was used to estimate the effect size and it is defined as the difference between two means $\bar{x_1}, \bar{x_2}$ divided by a standard deviation from the data s.

For each site an effect is added to the connectivity of W of the subjects, selected randomly ("pathological" group):

$$y_{i,j} = y_{i,j} + \mu. \tag{1}$$

The parameter μ is chosen to obtain a particular effect size (measured by the Cohen d)

$$d = \frac{\mu}{s_{i,j}}, \tag{2}$$

where $s_{i,j}$ is the standard deviation between region i and j for the reference population (mono-site). The significance of the difference between the control and 'treatment' group was assessed by a t-test in a linear model, including a covariate to model the motion. The study was repeated for various effect sizes (0 to 0.8 with a step of 0.01) with a p-value threshold of 0.001 on the t-test.

In order to introduce the same effect-size across the single-site and multi-site dataset we are taking the standard deviation from the single-site cohort as the reference. The connection $y_{i,j}$ of the randomly affected subjects ("treatment" group) are therefore calculated $y_{i,j} = y_{i,j} + d \times s_{i,j}$.

GLM model. In order to detec changes on each connection pair between groups artificialy created population in each simulation, a general linear model (GLM) was performed and the following confounding variables were modelled in the analysis: age, sex and frame displacement (FD). To account for site-specific bias $S - 1$ dummy-variables (binary vectors $1 \times S$) were added to the model with S being the total number of sites used in the study. The variables are corrected to have a zero mean across subjects, and an intercept (i.e. a column filled with 1) is added to $\mathbf{X}$ to capture the global average. The GLM relies on the following stochastic model Equation3.

$$\mathbf{Y} = \mathbf{X}\beta + \mathbf{V}\gamma + \mathbf{E}, \tag{3}$$

- $\mathbf{Y}$: $N \times 1$, connectivity value for the pair (i, j),

- $\mathbf{X}$: $N \times K$, explainable variables,
- β: $1 \times K$, regression values for each explainable variable,
- $\mathbf{V}$: $N \times S$, each column code for a site (0/1),
- γ: $1 \times S$, site average connectivity,
- $\mathbf{E}$: $N \times 1$, residual values from the regression,

with N the number of subjects, K the number of explainable variables and S the number of sites. Where β is an unknown $1 \times K$ vector of linear regression coefficients, γ is a $1 \times S$ vector of linear regression coefficients representing the contribution of each site and $\mathbf{E}$ is a $N \times 1$ random (noise) multivariate Gaussian variable. As data generated from different subjects are statistically independent, and under an homoscedasticity assumption, the regression coefficients β can be estimated with ordinary least squares.

Statistical detection and sensitivity. We relied on the following parametric assumptions on the noise E (1) that its rows are independent; (2) that each element follows a normal distribution with zero mean, and (3) that the variance of all elements are constant within a column, also called the homoscedasticity assumptions. As the data generated from different subjects are statistically independent the first assumption is reasonable. We tested the normality and homoscedasticity assumptions on real datasets. Under these parametric assumptions, the regression coefficients β and γ can be estimated with ordinary least squares and, for a given contrast (difference between the control and 'treatment' group) the significance of the contrast is assessed by a Student t-test.

The sensitivity of the test was evaluated by the average detection performance of all the samples (see Equation 4). For each sample b, we have a p-value p_b^* and the detection sensitivity is estimated by the probability of p_b^* being inferior to 0.001.

$$\frac{1}{B}\sum_{b=1}^{B}\left(p_b^* \leq 0.001\right). \tag{4}$$

Simulations scenarios. We first evaluated if a bias can be detected between sites. To do so we have computed the average connectome of each site along with the standard deviation matrix for each site. We then obatined the a mask of the significant differences between each sites (Student $t-test$ corrected for multiple comparison using FDR $\alpha = 0.05$) to have an idea of the size and spread of the functional bias.

For each experiment using real data, all effect size in the range 0 to 1.5 with a step of 0.01 were considered. The simulation were perfomed on 11 connections based on the literature review previously described in (TODO: cite the NATURE paper of Orban2015) reporting reproducible pair of regions reported to be affected by Alzheimer disease progression and displayed connectivity changes

between cognitively normal subjects and patient with dementia of the Alzheimer type. We implemented a series of experiments:

- We first checked how the total number of subject impact sensitivity using 3 different sample size (40, 80, 120) for an allocation ratio of $W = 0.5$,
- We then checked how the allocation ratio of participants W impact sensitivity using 3 different ratio ($W = 0.5, 0.3, 0.15$) for a total sample size of 120,
- We checked how the allocation ratio of participants W impact sensitivity using 3 different ratio ($W = 0.5, 0.3, 0.15$) for a total sample size of 120, including an interaction site-pathology effect of $d = 0.5$,
- We checked how the allocation ratio of participants $W = 0.3$ impact sensitivity using only 2 sites one large (80 subjects) and one small ($\sim$ 20 subjects) instead of the 7 sites previously used,

fully simulated data In order to obtain more control on each of the parameter of the simulation and simulate some configuration that were not possible to do with the real data (like the simulation of 2 medium size sites of of 40 and 60 subjects per site, and the size of the site effect) we have therefore used a synthetic model using only synthetic data and the average standard deviation of the Cambridge site connectivity.

For each experiment using synthetic data, all effect size in the range 0 to 1.5 with a step of 0.01 were considered. The simulation were perfomed using randomly generated values. All experiments show four scenarios,

For each experiment, all combinations of effect size in the grid without site-effect and with site-effect and the grid without interaction site-pathology and with interaction site-pathology were considered. We implemented a series of experiments:

- We first checked how 2 sites with respectively 50 subjects in each site with an allocation ratio of $W = 0.5$ in both sites are impacted in the 4 scenarios in term of sensitivity,
- We then checked how 2 sites with respectively 50 subjects in each site with an allocation ratio of $W = 0.7$ for the first site and $W = 0.3$ for the second site are impacted in the 4 scenarios in term of sensitivity,
- We checked how 2 sites (one small of 20 subjects and one large of 80 subjects) with an allocation ratio of $W = 0.5$ in both sites are impacted in the 4 scenarios in term of sensitivity,
- We checked how 2 sites (one small of 20 subjects and one large of 80 subjects) with an allocation ratio of $W = 0.7$ for the first site and $W = 0.3$ for the second site are impacted in the 4 scenarios in term of sensitivity,

- We checked how 2 sites (one small of 20 subjects and one large of 80 subjects) with an allocation ratio of $W = 0.7$ for the first site and $W = 0.3$ for the second site are impacted in the 4 scenarios in term of sensitivity,
- We checked how 50 sites (with a number of sumbject per site randomly assigned between 2 and 15) with an allocation ratio W randomly assigned between 0.1 and 0.9 for each sites are impacted in term of sensitivity for 2 scenarios (without and with interaction site pathology),

3. Results

3.1. Inter-site variability

The first assessment perform on the dataset was to verify the distribution of the variance in functional connectivity among each site and across sites in order to see if they are of the same order of magnitude or not. This analysis of Figure 1 shows the distribution of the standard deviation in connectivity across subjects (the distribution is over the full brain connectome, with several 1000s connections) at the 8 sites against the inter-sites standard deviation of connectomes (average at each site). As we can see the inter-site (between-site) variability is smaller than the intra-site (between subjects) variability, in fact the amplitude of inter-site bias is about 3-fold smaller than the within-site standard deviation (red ~ 0.06 vs. orange ~ 0.18).

In order to verify how spatial structure vary across sites the average standard deviation and the average connectivity map of the DMN were extracted for each site and reported in Figure 2. As we can see in the intersection between two sites the difference in average connectivity between-sites is illustrated (red set of brain cuts). First the mean DMN at each site is consistent with the expected spatial distribution reported in other studies (Damoiseaux et al., 2006; Dansereau et al., 2014; Yan et al., 2013b). The most salient changes between-sites are located in the mesio-frontal region associated with the anterior part of the DMN. In order to verify if significant changes are not only found in the DMN we have computed the entier connectome in order to obtain the other connectivity patterns and the findings can be generalized to the full connectome see Figure 3.

3.2. Simulation on real data

In order to evaluate the impact of multisite configuration on our ability to detect changes in rs-functional connectivity studies we performed various simulation on real fMRI data. For each site and each sample, B of the subjects were randomly assigned to a 'treatment' group. For the subjects in this group, a value was added to achieve a given relative effect size expressed in Cohen's d. The significance of the difference between the control and 'treatment' group was assessed by a t-test in a linear model. To account for site-specific bias we have included dummy variables in the GLM model. The study was repeated for various effect sizes (0 to 1.5 with a step of 0.01) at a threshold of 0.001 on the p-value.

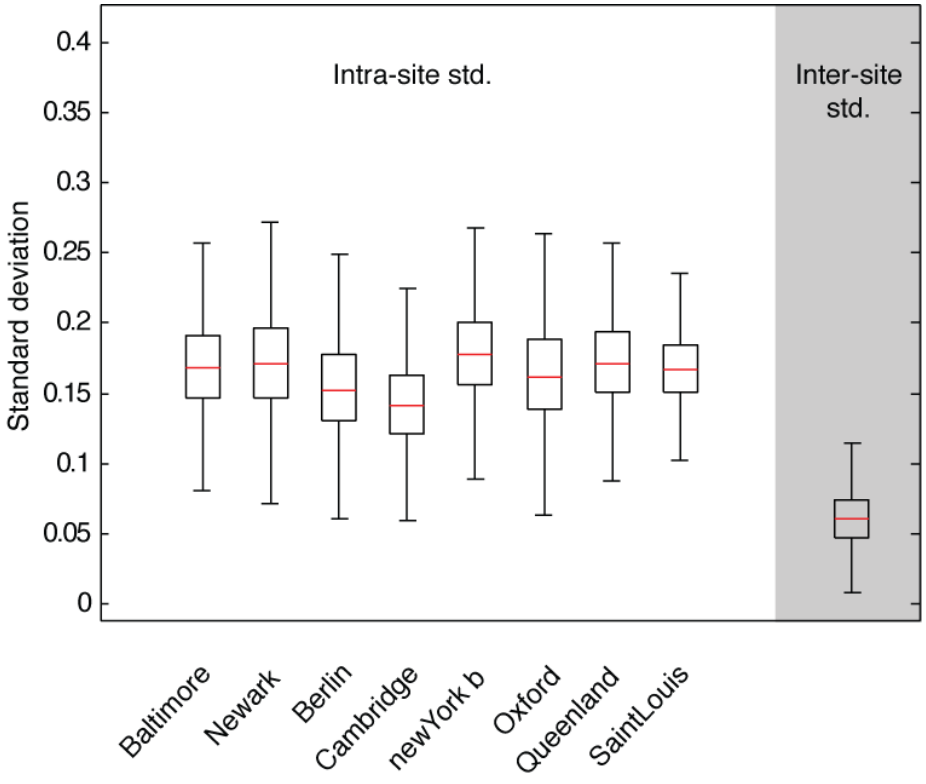

Figure 1: Distribution of intra-site (between-subject) standard deviation vs. inter-site (between-site) standard deviation, based on the standard deviation of the connectivity matrices from 8 sites from the 1000 functional connectome dataset.

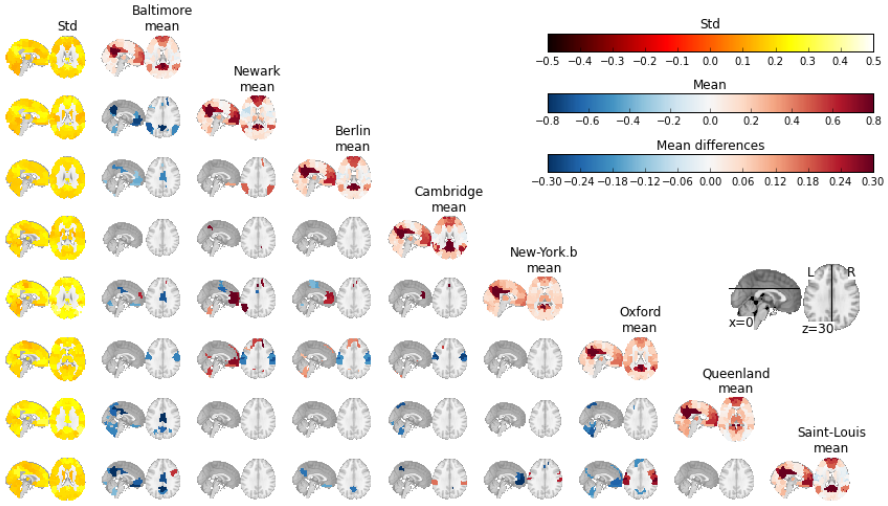

Figure 2: Functional connectivity maps of the default-mode network at multiple sites. The average connectivity map are shown on the diagonal. The standard deviation across subjects and within site is shown on the first column. Each off-diagonal block represent the significant differences between the average functional connectivity maps between two sites (called the inter-site bias).

Figure 4 show the pair of regions used in (TODO ORBAN2015) as candidate marker for functional connectivity changes in Alzheimer disease based on a literature review. We will use the correlation between those regions to estimate the variability across subject and induce some effect in our simulations.

In Figure 5 we show the effect of the sample size on the detection power. As expected we are able to detect smaller and smaller effect size as we increase the sample size. For an effect size of 1 which is considered a large effect we are able to detect significant changes in only 20% of the cases at 40 subjects, 80% at 80 subjects and almost 95% at 120% subjects.

Figure 6 show the effect of debalancing the two groups at various ratio (50%-50% , 30%-70% and 15%-85%) for a total sample size of 120 subjects. Has the debalancing increase our ability to detect effect is diminished. As an example for an effect size of 1 we would detect the effect in 95% of the cases in a 50 balanced scenario, this would go down to 90% in a 30%-70% scenario and to 60% in a 15%-85% debalancing.

Figure 7 show the effect of debalancing the two groups at various ratio (50%-50% , 30%-70% and 15%-85%) with an interaction site-pathology (0.5 Cohen's d) for a total sample size of 120 subjects. Has the debalancing increase our ability to detect effect is diminished. As an example for an effect size of 1 we would detect the effect in 98% of the cases in a 50 balanced scenario, this would go down to 95% in a 30%-70% scenario and to 75% in a 15%-85% debalancing.

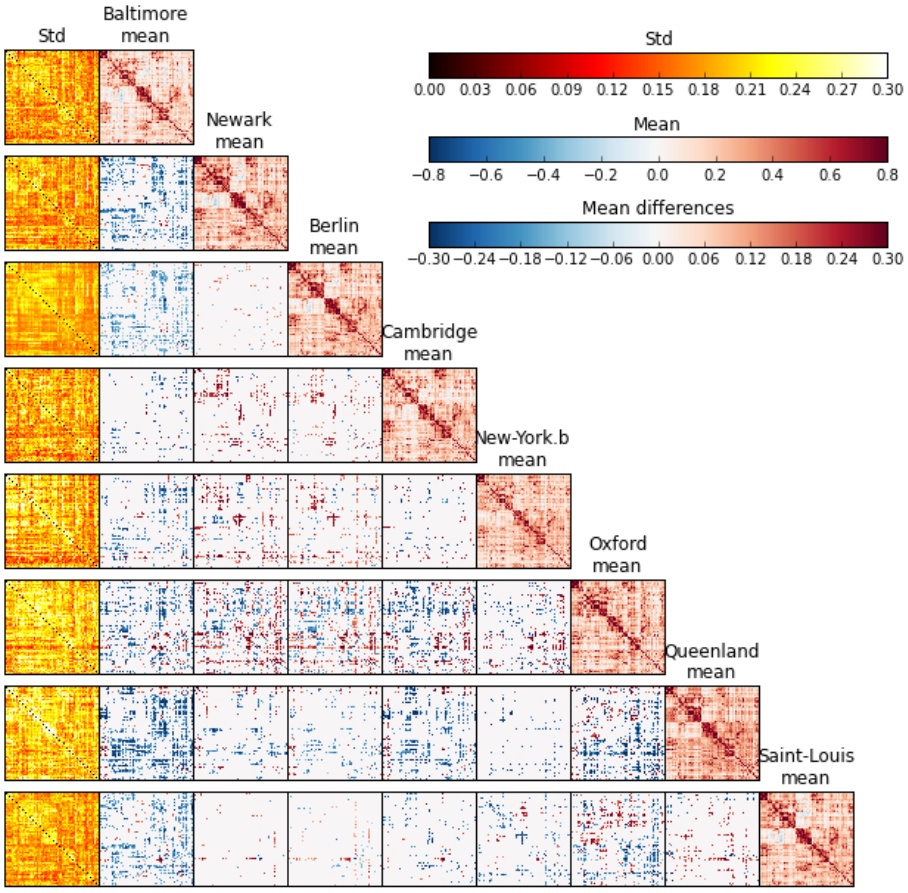

Figure 3: Functional connectome for multiple sites. The average connectome of 8 sites (Baltimore, Newark, Berlin, Cambridge, New-Yorkb, Oxford, Queenland and SaintLouis at 3T) are shown on the diagonal. The standard deviation across subjects and within site is shown on the first column. Each off-diagonal block represent the absolute difference between the average functional connectivity maps between two sites (called the inter-site bias).

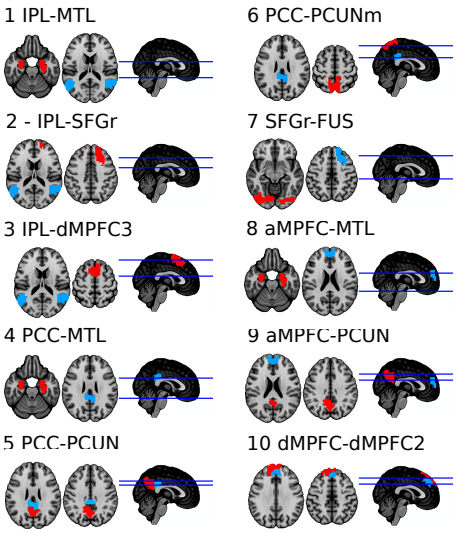

Figure 4: Connexions pair based on a literature review.

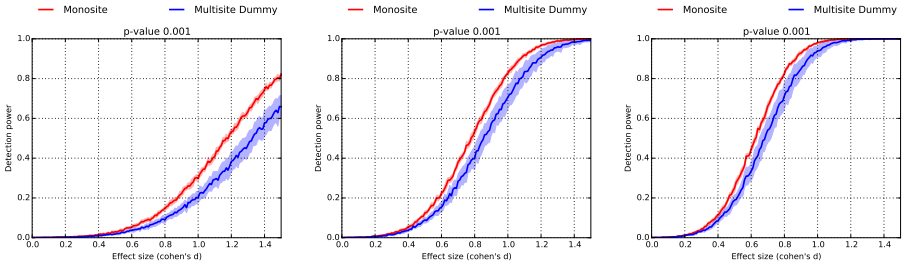

40 subjects 80 subjects 120 subjects

Figure 5: Simulation on real data, detection power of two groups balanced 50%-50% between 7 sites. Two scenarios, 1) monosite and 2) multisite 7 sites with correction for multisite differences using dummy variables. Each plot show the detection power in function of the effect size for 3 different sample size 40, 80 and 120 subjects in total.

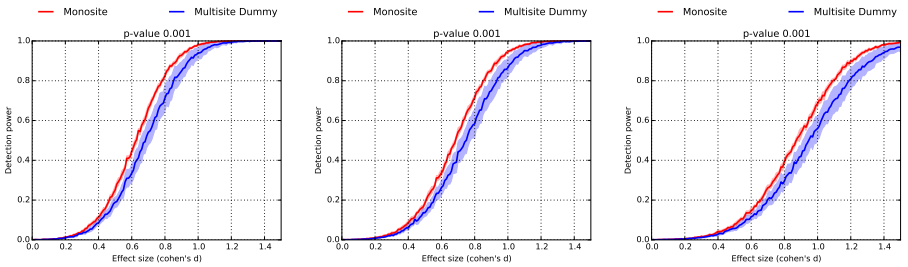

Debalancing 50% Debalancing 30% Debalancing 15%

Figure 6: Simulation on real data, detection power of two groups for a total of 120 subject between 7 sites. All plot show two scenarios, 1) monosite and 2) multisite 7 sites with correction for multisite differences using dummy variables.

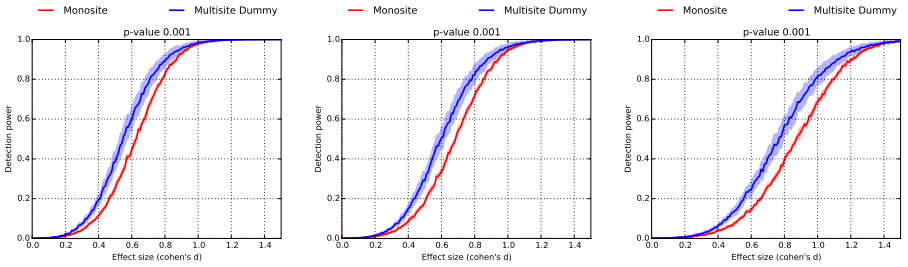

Debalancing 50% Debalancing 30% Debalancing 15%

Figure 7: Simulation on real data, detection power of two groups for a total of 120 subject between 7 sites with a site-pathology interaction at 0.5. All plot show two scenarios, 1) monosite and 2) multisite 7 sites with correction for multisite differences using dummy variables.

The particularity of this experiment is the fact that the multisite configuration perform better then the single site meanning that it is better to have interaction of various amplitude across small sites than an average interaction on one large site.

Figure 8 show a scenario of two site one large (80 subjects) and one small ($\sim$ 20 subjects) unbalanced at 30%-70% and the inverse. As we can see the multisite configuration is as good as the monosite.

Using this Monte-Carlo simulations we have shown that the power of detecting an effect is marginally affected by the site acquisition configuration (single site or multi-site) when the sites are balanced in term of the amount of subject with and without the effect.

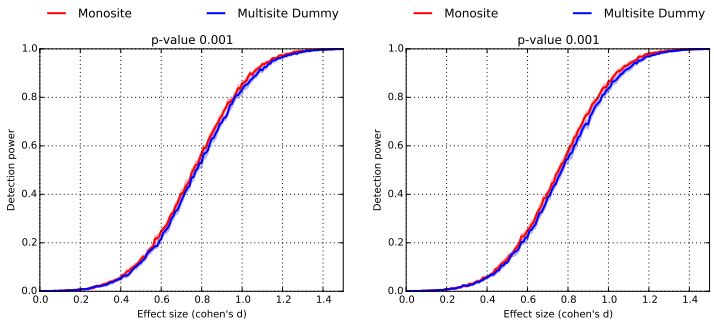

Figure 8: Simulation on real data, detection power of two groups for a total of 100 subject between 2 sites, one small site of 20 subjects and one large of 80 subjects. All plot show two scenarios, 1) monosite and 2) multisite 2 sites with correction for multisite differences using dummy variables. Simulation of the detection power of two groups balanced 30% and 70% between 2 sites.

3.3. Simulation on synthetic data

In order to obtain more control on each of the parameter of the simulation and simulate some configuration that were not possible to do with the real data (like the simulation of 2 medium size sites of of 40 and 60 subjects per site, and the size of the site effect) we have therefore used a synthetic model using only synthetic data and the average standard deviation of the Cambridge site connectivity. All plots show four scenarios: The top left plot represent the two configurations one monosite and two sites with correction for multisite differences using dummy variables without site effect. Has expected there is no difference between using 1 large site than combining two site of half the size. The plot on the upper right corner represent the detection power when we apply a site effect on balanced sites, here again not much differences an additive effect is fully compensated by the dummy variables corrective method. the lower left plot represent no site effect but an interaction between site and pathology. An the last plot on the lower right corner show the detection power with a site effect of 0.5 and a interation site pathology.

Figure 13 show the same configuration but the sample size are inverted. Has we can see we have the same pattern as in the real data with...

Figure 14 show a more realistic case in clinical trials where the number of scanning sites is very large and the number of subjects per site is small. There is usually no control on the exact balancing of those sites therefore we have randomly assign debalancing for each site (between 10% and 90%) and have randomly assigned a number of subject to each site (between 2 and 15 subjects).

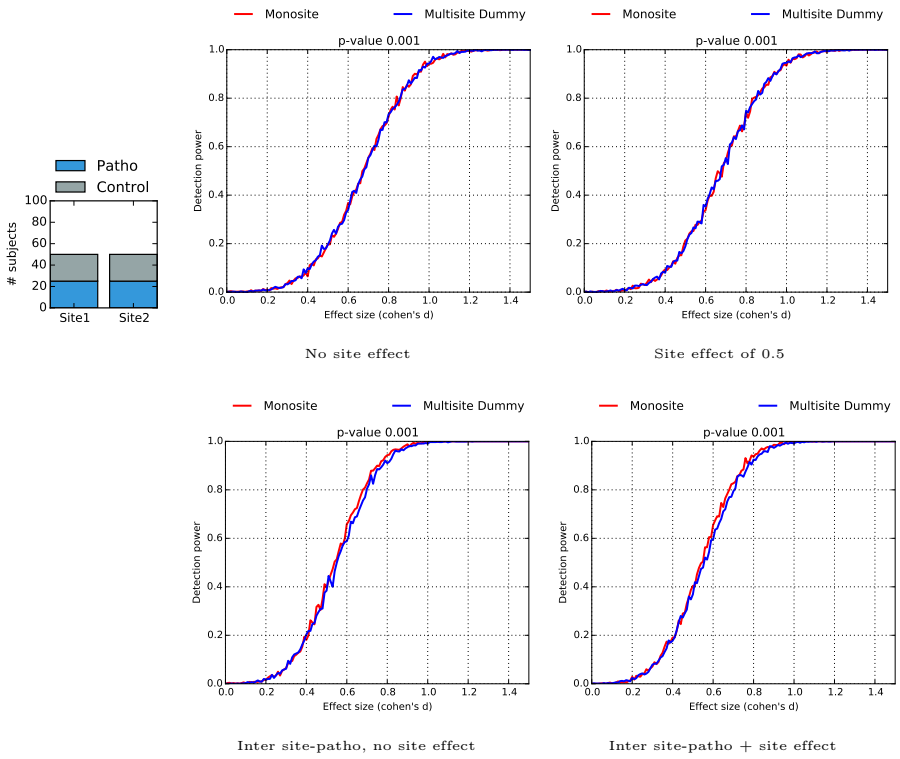

Figure 9: Simulation of the detection power of two groups balanced 50%-50% between two sites. All plots show four scenarios in two configuration one monosite and two sites with correction for multisite differences using dummy variables. The first column represent scenarios without site effect and the second column show with a site effect the first row show simulation with out interaction site-pathology and the second row show with interaction.

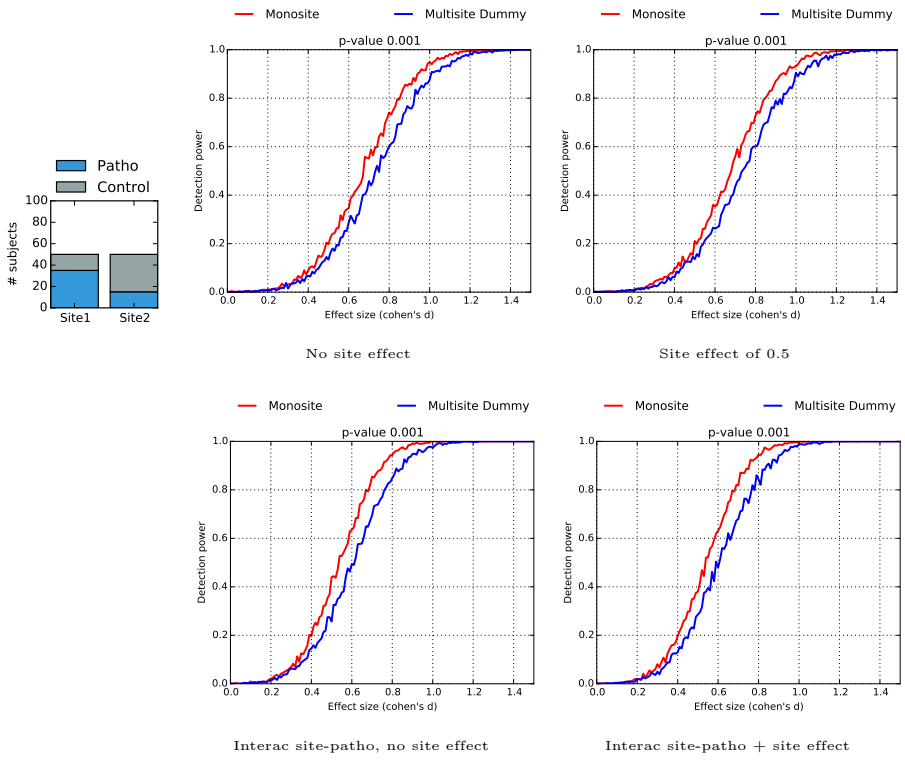

Figure 10: Simulation of the detection power of two groups unbalanced 70%-30% between two sites. All plots show four scenarios in two configuration one monosite and two sites with correction for multisite differences using dummy variables. The first column represent scenarios without site effect and the second column show with a site effect the first row show simulation with out interaction site-pathology and the second row show with interaction.

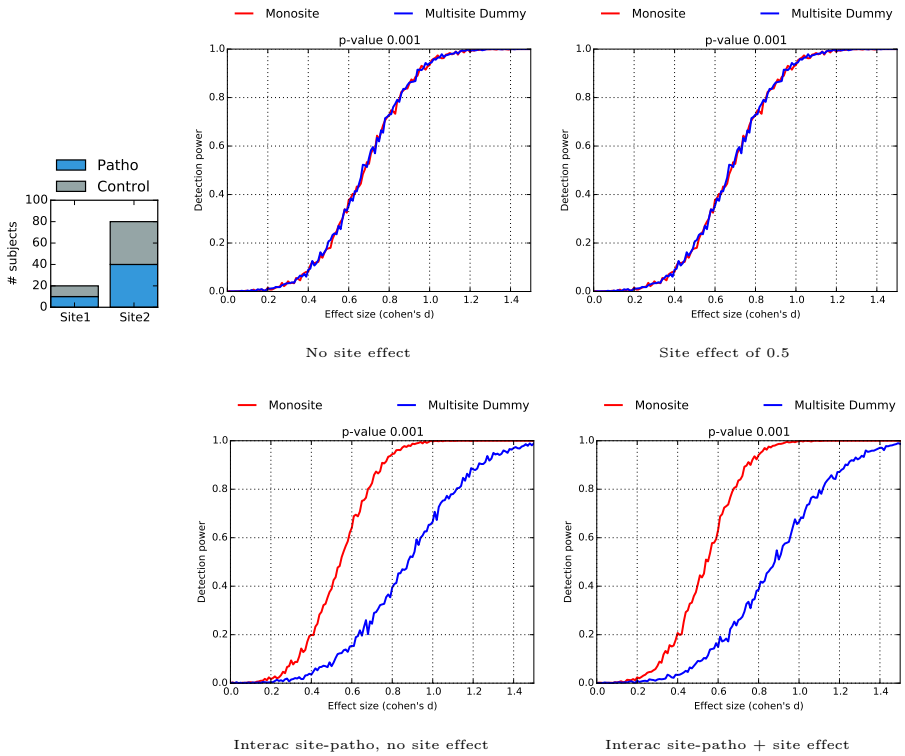

Figure 11: Simulation of the detection power of two groups unbalanced 50%-50% between two sites, one small site of 20 subjects and one large of 80 subjects. All plots show four scenarios in two configuration one monosite and two sites with correction for multisite differences using dummy variables. The first column represent scenarios without site effect and the second column show with a site effect the first row show simulation with out interaction site-pathology and the second row show with interaction.

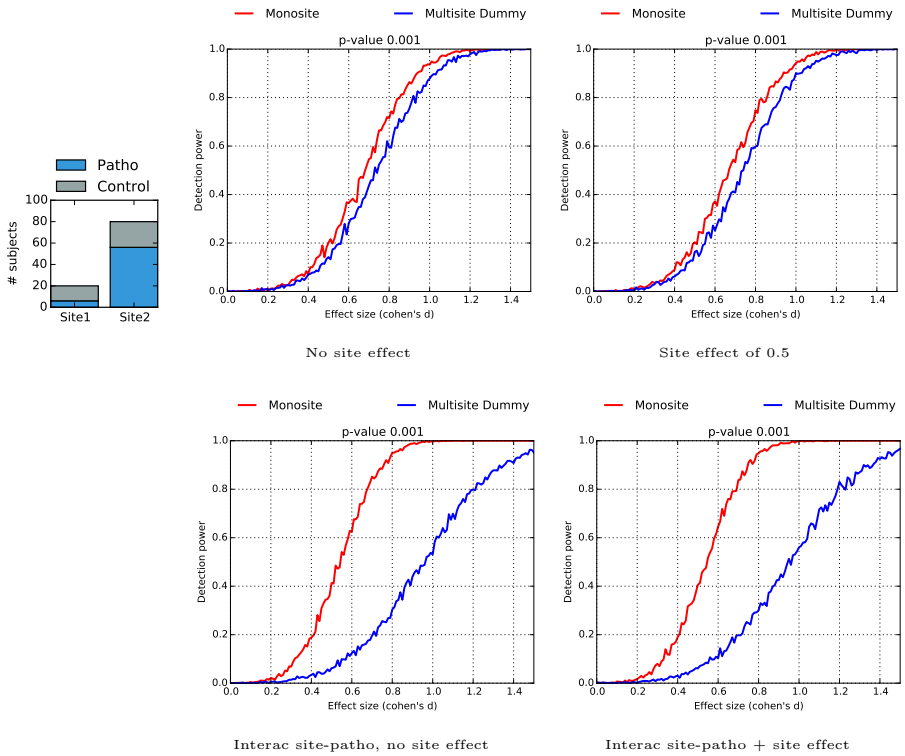

Figure 12: Simulation of the detection power of two groups unbalanced 70%-30% between two sites, one small site of 20 subjects and one large of 80 subjects. All plots show four scenarios in two configuration one monosite and two sites with correction for multisite differences using dummy variables. The first column represent scenarios without site effect and the second column show with a site effect the first row show simulation with out interaction site-pathology and the second row show with interaction.

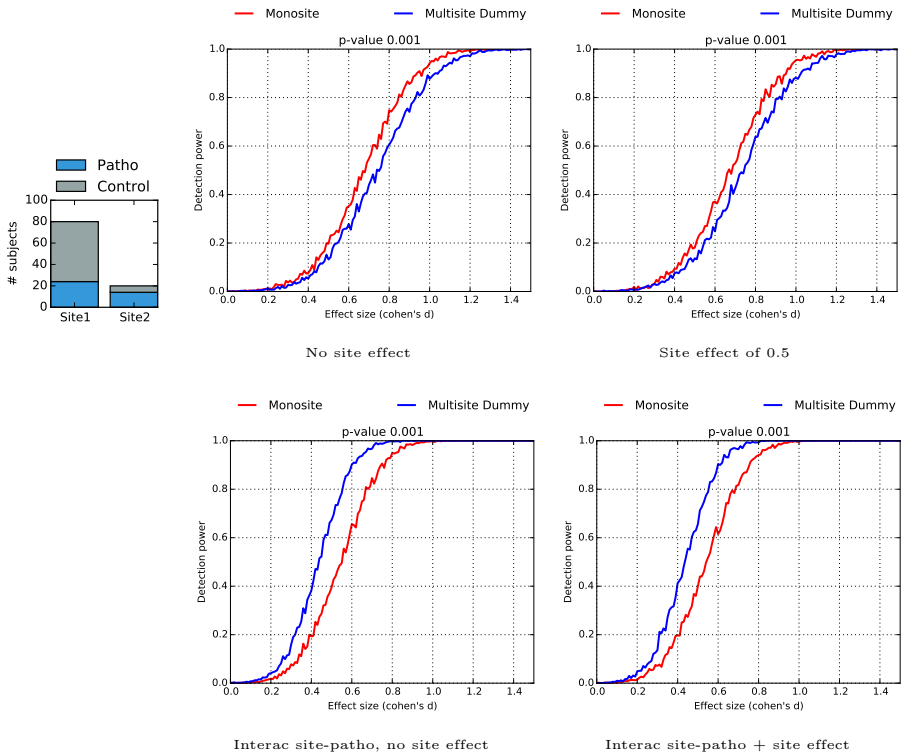

Figure 13: Simulation of the detection power of two groups unbalanced 70%-30% between two sites, one small site of 20 subjects and one large of 80 subjects. All plots show four scenarios in two configuration one monosite and two sites with correction for multisite differences using dummy variables. The first column represent scenarios without site effect and the second column show with a site effect the first row show simulation with out interaction site-pathology and the second row show with interaction.

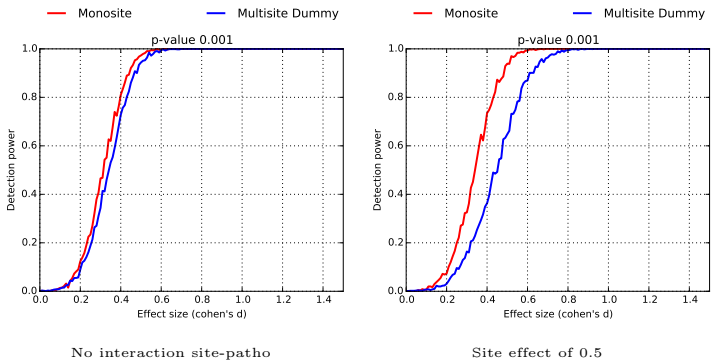

Figure 14: Simulation of the detection power of two groups balanced randomly between 10%-90% between 50 sites, the number of subject per site is randomly assigned between 2 and 15. All plot show four scenario, one monosite and two sites with correction for multisite differences using dummy variables. The plots show the detection power when the variability is greater in one side then the other for the pathology group (twice the reference variability in one site and half the reference variability in the other one).

4. Discussion

Connectivity bias that can impact interpretation.

Type of scanner most of them are Siemens we may have more variability if combining various brand

Talk about the impact in small acquisition 40 subjects total and the importance of pooling data among PI.

Talk about the impact in clinical trial and best practice.
most of the time we cannot correct for site with one population only or with too few subjects per site. Although these kind of multisite studies generally sum-up to large dataset of more than 200 subjects. has we demonstrated in the synthetic simulation such configuration are comparable to single site analysis for this range of sample size.

It is better to have interaction of various amplitude across small sites than an average interaction on one large site

5. Conclusion

6. Acknowledgments

Parts of this work were presented at the 2013 annual meetings of the organization for human brain mapping (**?**), as well as the Alzheimer's Association

International Conference (AAIC) (2013) (Boston) (**?**). The authors are grateful to the members of the 1000 functional connectome consortium for publicly releasing there dataset. The computational resources used to perform the data analysis were provided by ComputeCanada[6] and CLUMEQ[7], which is funded in part by NSERC (MRS), FQRNT, and McGill University. This project was funded by NSERC grant number RN000028, a salary award from "Fonds de recherche du Québec – Santé" to PB as well as a salary award by the Canadian Institute of Health Research to CD.

References

Bellec, P., Feb. 2006. Longitudinal study of large-scale networks in the human brain using fMRI : Methods and application to motor skill learning. Ph.D. thesis, Université Paris XI, Orsay, Paris.
URL `http://exocet.imed.jussieu.fr/~{}pbellec/data/these_bellec.pdf`

Bellec, P., Carbonell, F., Perlbarg, V., Evans, A. C., 2010a. A neuroimaging analysis kit for Octave and Matlab.
URL `http://code.google.com/p/niak/`

Bellec, P., Rosa-Neto, P., Lyttelton, O. C., Benali, H., Evans, A. C., Jul. 2010b. Multi-level bootstrap analysis of stable clusters in resting-state fMRI. NeuroImage 51 (3), 1126–1139.
URL `http://dx.doi.org/10.1016/j.neuroimage.2010.02.082`

Biswal, B. B., Mennes, M., Zuo, X.-N. N., Gohel, S., Kelly, C., Smith, S. M., Beckmann, C. F., Adelstein, J. S., Buckner, R. L., Colcombe, S., Dogonowski, A.-M. M., Ernst, M., Fair, D., Hampson, M., Hoptman, M. J., Hyde, J. S., Kiviniemi, V. J., Kötter, R., Li, S.-J. J., Lin, C.-P. P., Lowe, M. J., Mackay, C., Madden, D. J., Madsen, K. H., Margulies, D. S., Mayberg, H. S., McMahon, K., Monk, C. S., Mostofsky, S. H., Nagel, B. J., Pekar, J. J., Peltier, S. J., Petersen, S. E., Riedl, V., Rombouts, S. A., Rypma, B., Schlaggar, B. L., Schmidt, S., Seidler, R. D., Siegle, G. J., Sorg, C., Teng, G.-J. J., Veijola, J., Villringer, A., Walter, M., Wang, L., Weng, X.-C. C., Whitfield-Gabrieli, S., Williamson, P., Windischberger, C., Zang, Y.-F. F., Zhang, H.-Y. Y., Castellanos, F. X., Milham, M. P., Mar. 2010. Toward discovery science of human brain function. Proceedings of the National Academy of Sciences of the United States of America 107 (10), 4734–4739.
URL `http://dx.doi.org/10.1073/pnas.0911855107`

Carbonell, F., Bellec, P., Shmuel, A., Feb 2014. Quantification of the impact of a confounding variable on functional connectivity confirms anti-correlated

[6] `https://computecanada.org/`
[7] `http://www.clumeq.mcgill.ca/`

networks in the resting-state. Neuroimage 86, 343–353.
URL http://dx.doi.org/10.1016/j.neuroimage.2013.10.013

Cheng, W., Palaniyappan, L., Li, M., Kendrick, K. M., Zhang, J., Luo, Q., Liu, Z., Yu, R., Deng, W., Wang, Q., Ma, X., Guo, W., Francis, S., Liddle, P., Mayer, A. R., Schumann, G., Li, T., Feng, J., May 2015. Voxel-based, brain-wide association study of aberrant functional connectivity in schizophrenia implicates thalamocortical circuitry. Npj Schizophrenia 1, –.
URL http://dx.doi.org/10.1038/npjschz.2015.16

Collins, D. L., Zijdenbos, A. P., Kollokian, V., Sled, J. G., Kabani, N. J., Holmes, C. J., Evans, A. C., Jun. 1998. Design and construction of a realistic digital brain phantom. IEEE Trans Med Imaging 17 (3), 463–468.
URL http://view.ncbi.nlm.nih.gov/pubmed/9735909

Damoiseaux, J. S., Prater, K. E., Miller, B. L., Greicius, M. D., Apr. 2012. Functional connectivity tracks clinical deterioration in Alzheimer's disease. Neurobiology of Aging 33 (4), 828.e19–828.e30.
URL http://dx.doi.org/10.1016/j.neurobiolaging.2011.06.024

Damoiseaux, J. S., Rombouts, S. A. R. B., Barkhof, F., Scheltens, P., Stam, C. J., Smith, S. M., Beckmann, C. F., Sep. 2006. Consistent resting-state networks across healthy subjects. Proceedings of the National Academy of Sciences 103 (37), 13848–13853.
URL http://dx.doi.org/10.1073/pnas.0601417103

Dansereau, C., Bellec, P., Lee, K., Pittau, F., Gotman, J., Grova, C., 2014. Detection of abnormal resting-state networks in individual patients suffering from focal epilepsy: An initial step toward individual connectivity assessment. Frontiers in Neuroscience 8 (419).
URL http://www.frontiersin.org/brain_imaging_methods/10.3389/fnins.2014.00419/abstract

De Luca, M., Beckmann, C. F., De Stefano, N., Matthews, P. M., Smith, S. M., Feb. 2006. fMRI resting state networks define distinct modes of long-distance interactions in the human brain. NeuroImage 29 (4), 1359–1367.
URL http://dx.doi.org/10.1016/j.neuroimage.2005.08.035

Desmond, J., Glover, G., Aug. 2002. Estimating sample size in functional mri (fmri) neuroimaging studies: Statistical power analyses. Journal of Neuroscience Methods 118 (2), 115–128.
URL http://dx.doi.org/10.1016/s0165-0270(02)00121-8

Edward, V., Windischberger, C., Cunnington, R., Erdler, M., Lanzenberger, R., Mayer, D., Endl, W., Beisteiner, R., Nov 2000. Quantification of fmri artifact reduction by a novel plaster cast head holder. Hum Brain Mapp 11 (3), 207–213.

Elliott, M. R., Bowtell, R. W., Morris, P. G., Jun 1999. The effect of scanner sound in visual, motor, and auditory functional mri. Magn Reson Med 41 (6), 1230–1235.

Fair, D. A., Nigg, J. T., Iyer, S., Bathula, D., Mills, K. L., Dosenbach, N. U. F., Schlaggar, B. L., Mennes, M., Gutman, D., Bangaru, S., Buitelaar, J. K., Dickstein, D. P., Martino, A. D., Kennedy, D. N., Kelly, C., Luna, B., Schweitzer, J. B., Velanova, K., Wang, Y.-F., Mostofsky, S., Castellanos, F. X., Milham, M. P., 2012. Distinct neural signatures detected for adhd subtypes after controlling for micro-movements in resting state functional connectivity mri data. Front Syst Neurosci 6, 80.
URL http://dx.doi.org/10.3389/fnsys.2012.00080

Fonov, V., Evans, A. C., Botteron, K., Almli, C. R., McKinstry, R. C., Collins, D. L., Brain Development Cooperative Group, Jan. 2011. Unbiased average age-appropriate atlases for pediatric studies. NeuroImage 54 (1), 313–327.
URL http://dx.doi.org/10.1016/j.neuroimage.2010.07.033

Fox, M. D., Zhang, D., Snyder, A. Z., Raichle, M. E., Jun 2009. The global signal and observed anticorrelated resting state brain networks. J Neurophysiol 101 (6), 3270–3283.
URL http://dx.doi.org/10.1152/jn.90777.2008

Friedman, L., Glover, G., Jun. 2006. Report on a multicenter fmri quality assurance protocol. Journal of magnetic resonance imaging : JMRI 23 (6), 827–839.
URL http://dx.doi.org/10.1002/jmri.20583

Friedman, L., Glover, G., Consortium, T. F., Nov. 2006. Reducing interscanner variability of activation in a multicenter fmri study: Controlling for signal-to-fluctuation-noise-ratio (sfnr) differences. NeuroImage 33 (2), 471–481.
URL http://dx.doi.org/10.1016/j.neuroimage.2006.07.012

Giove, F., Gili, T., Iacovella, V., Macaluso, E., Maraviglia, B., Oct. 2009. Images-based suppression of unwanted global signals in resting-state functional connectivity studies. Magnetic resonance imaging 27 (8), 1058–1064.
URL http://dx.doi.org/10.1016/j.mri.2009.06.004

Goveas, J. S., Xie, C., Ward, B. D., Wu, Z., Li, W., Franczak, M., Jones, J. L., Antuono, P. G., Li, S.-J. J., Oct. 2011. Recovery of hippocampal network connectivity correlates with cognitive improvement in mild Alzheimer's disease patients treated with donepezil assessed by resting-state fMRI. Journal of magnetic resonance imaging : JMRI 34 (4), 764–773.
URL http://dx.doi.org/10.1002/jmri.22662

He, Y., Chen, Z., Gong, G., Evans, A., Aug. 2009. Neuronal networks in Alzheimer's disease. The Neuroscientist : a review journal bringing neurobiology, neurology and psychiatry 15 (4), 333–350.
URL http://dx.doi.org/10.1177/1073858409334423

Jafri, M. J. J., Pearlson, G. D. D., Stevens, M., Calhoun, V. D. D., Nov. 2007. A method for functional network connectivity among spatially independent resting-state components in schizophrenia. Neuroimage.
URL http://dx.doi.org/10.1016/j.neuroimage.2007.11.001

Kelly, C., Biswal, B., Craddock, C., Castellanos, X., Milham, M., Mar. 2012. Characterizing variation in the functional connectome: promise and pitfalls. Trends in Cognitive Sciences 16 (3), 181–188.
URL http://dx.doi.org/10.1016/j.tics.2012.02.001

Lu, Y., Jiang, T., Zang, Y., Sep. 2003. Region growing method for the analysis of functional MRI data. NeuroImage 20 (1), 455–465.
URL http://dx.doi.org/10.1016/S1053-8119(03)00352-5

Lund, T. E., Madsen, K. H., Sidaros, K., Luo, W.-L., Nichols, T. E., Jan. 2006. Non-white noise in fMRI: does modelling have an impact? NeuroImage 29 (1), 54–66.
URL http://dx.doi.org/10.1016/j.neuroimage.2005.07.005

Marrelec, G., Bellec, P., Krainik, A., Duffau, H., Pélégrini-Issac, M., Lehéricy, S., Benali, H., Doyon, J., Feb. 2008. Regions, systems, and the brain: Hierarchical measures of functional integration in fMRI. Medical image analysis.
URL http://dx.doi.org/10.1016/j.media.2008.02.002

Mueller, S. G., Weiner, M. W., Thal, L. J., Petersen, R. C., Jack, C., Jagust, W., Trojanowski, J. Q., Toga, A. W., Beckett, L., Nov 2005. The alzheimer's disease neuroimaging initiative. Neuroimaging Clin N Am 15 (4), 869–77, xi–xii.
URL http://dx.doi.org/10.1016/j.nic.2005.09.008

Murphy, K., Birn, R. M., Handwerker, D. A., Jones, T. B., Bandettini, P. A., Feb. 2009. The impact of global signal regression on resting state correlations: are anti-correlated networks introduced? NeuroImage 44 (3), 893–905.
URL http://dx.doi.org/10.1016/j.neuroimage.2008.09.036

Nielsen, J., Zielinski, B., Fletcher, T., Alexander, A., Lange, N., Bigler, E., Lainhart, J., Anderson, J., 2013. Multisite functional connectivity mri classification of autism: Abide results. Frontiers in human neuroscience 7, –.
URL http://view.ncbi.nlm.nih.gov/pubmed/24093016

Power, J. D., Barnes, K. A., Snyder, A. Z., Schlaggar, B. L., Petersen, S. E., Feb. 2012. Spurious but systematic correlations in functional connectivity MRI networks arise from subject motion. NeuroImage 59 (3), 2142–2154.
URL http://dx.doi.org/10.1016/j.neuroimage.2011.10.018

Power, J. D., Mitra, A., Laumann, T. O., Snyder, A. Z., Schlaggar, B. L., Petersen, S. E., Jan. 2014. Methods to detect, characterize, and remove motion artifact in resting state fMRI. NeuroImage 84, 320–341.
URL http://dx.doi.org/10.1016/j.neuroimage.2013.08.048

Rorden, C., Karnath, H.-O., Bonilha, L., Jul 2007. Improving lesion-symptom mapping. J Cogn Neurosci 19 (7), 1081–1088.
URL http://dx.doi.org/10.1162/jocn.2007.19.7.1081

Saad, Z. S., Gotts, S. J., Murphy, K., Chen, G., Jo, H. J. J., Martin, A., Cox, R. W., 2012. Trouble at rest: how correlation patterns and group differences become distorted after global signal regression. Brain connectivity 2 (1), 25–32.
URL http://dx.doi.org/10.1089/brain.2012.0080

Thirion, B., Dodel, S., Poline, J. B., Jan. 2006. Detection of signal synchronizations in resting-state fMRI datasets. Neuroimage 29 (1), 321–327.
URL http://dx.doi.org/10.1016/j.neuroimage.2005.06.054

Tomasi, D., Volkow, N. D., May 2010. Functional connectivity density mapping. Proceedings of the National Academy of Sciences 107 (21), 9885–9890.
URL http://dx.doi.org/10.1073/pnas.1001414107

Tzourio-Mazoyer, N., Landeau, B., Papathanassiou, D., Crivello, F., Etard, O., Delcroix, N., Mazoyer, B., Joliot, M., Jan. 2002. Automated anatomical labeling of activations in SPM using a macroscopic anatomical parcellation of the MNI MRI single-subject brain. NeuroImage 15 (1), 273–289.
URL http://dx.doi.org/10.1006/nimg.2001.0978

Van Dijk, K. R., Hedden, T., Venkataraman, A., Evans, K. C., Lazar, S. W., Buckner, R. L., Jan. 2010. Intrinsic functional connectivity as a tool for human connectomics: theory, properties, and optimization. Journal of neurophysiology 103 (1), 297–321.
URL http://dx.doi.org/10.1152/jn.00783.2009

Vanhoutte, G., Verhoye, M., der Linden, A. V., May 2006. Changing body temperature affects the t2* signal in the rat brain and reveals hypothalamic activity. Magn Reson Med 55 (5), 1006–1012.
URL http://dx.doi.org/10.1002/mrm.20861

Wang, K., Liang, M., Wang, L., Tian, L., Zhang, X., Li, K., Jiang, T., Oct. 2007. Altered functional connectivity in early Alzheimer's disease: a resting-state fMRI study. Human brain mapping 28 (10), 967–978.
URL http://dx.doi.org/10.1002/hbm.20324

Wang, L., Zang, Y., He, Y., Liang, M., Zhang, X., Tian, L., Wu, T., Jiang, T., Li, K., Jun. 2006. Changes in hippocampal connectivity in the early stages of Alzheimer's disease: evidence from resting state fMRI. NeuroImage 31 (2), 496–504.
URL http://dx.doi.org/10.1016/j.neuroimage.2005.12.033

Yan, C., Liu, D., He, Y., Zou, Q., Zhu, C., Zuo, X., Long, X., Zang, Y., May 2009. Spontaneous Brain Activity in the Default Mode Network Is Sensitive to Different Resting-State Conditions with Limited Cognitive Load. PLoS ONE

4 (5), e5743+.
URL http://dx.doi.org/10.1371/journal.pone.0005743

Yan, C.-G., Cheung, B., Kelly, C., Colcombe, S., Craddock, R. C., Di Martino, A., Li, Q., Zuo, X.-N., Castellanos, F. X., Milham, M. P., Aug. 2013a. A comprehensive assessment of regional variation in the impact of head micromovements on functional connectomics. NeuroImage 76, 183–201.
URL http://dx.doi.org/10.1016/j.neuroimage.2013.03.004

Yan, C.-G. G., Craddock, C. C., Zuo, X.-N. N., Zang, Y.-F. F., Milham, M. P., Oct. 2013b. Standardizing the intrinsic brain: towards robust measurement of inter-individual variation in 1000 functional connectomes. NeuroImage 80, 246–262.
URL http://view.ncbi.nlm.nih.gov/pubmed/23631983

Zhang, H., Wang, S., Xing, J., Liu, B., Ma, Z., Yang, M., Zhang, Z., Teng, G., Jan. 2009. Detection of PCC functional connectivity characteristics in resting-state fMRI in mild Alzheimer's disease. Behavioural Brain Research 197 (1), 103–108.
URL http://dx.doi.org/10.1016/j.bbr.2008.08.012

Zhang, H., Zuo, X.-N., Ma, S.-Y., Zang, Y.-F., Milham, M. P., Zhu, C.-Z., Mar. 2010. Subject Order-Independent Group ICA (SOI-GICA) for Functional MRI Data Analysis. NeuroImage.
URL http://dx.doi.org/10.1016/j.neuroimage.2010.03.039

Zijdenbos, A. P., Forghani, R., Evans, A. C., Oct. 2002. Automatic "pipeline" analysis of 3-D MRI data for clinical trials: application to multiple sclerosis. IEEE Transactions on Medical Imaging 21 (10), 1280–1291.
URL http://dx.doi.org/10.1109/TMI.2002.806283

Zuo, X.-N., Xu, T., Jiang, L., Yang, Z., Cao, X.-Y., He, Y., Zang, Y.-F., Castellanos, F. X., Milham, M. P., Oct. 2012. Toward reliable characterization of functional homogeneity in the human brain: Preprocessing, scan duration, imaging resolution and computational space. NeuroImage.
URL http://dx.doi.org/10.1016/j.neuroimage.2012.10.017

Supplementary Material – Feasibility of multi-centric fMRI connectivity studies of Alzheimer's disease

Submitted to Neuroimage.

C. Dansereau[1,2], C. Risterucci[3], E. Merlo Pich[3], D. Arnold[4], P. Bellec[1,2]

[1]Functional Neuroimaging Unit, Centre de Recherche de l'Institut Universitaire de Gériatrie de Montréal
[2]Department of Computer Science and Operations Research, University of Montreal, Montreal, Quebec, Canada
[3]F. Hoffmann-La Roche Ldt., Basel, Switzerland
[4]NeuroRx, Montreal, Quebec, Canada

For all questions regarding the paper, please address correspondence to Pierre Bellec, CRIUGM, 4545 Queen Mary, Montreal, QC, H3W 1W5, Canada. Email: pierre.bellec (at) criugm.qc.ca.

Literature review: Alzheimers disease and resting-state fMRI

- Zhang et al. (2009) used functional connectivity maps with a seed in the posterior cingulate cortex (PCC) to explore the differences between a group of elderly cognitively normal subjects (CNE, n=16) and patients with a mild dementia of the Alzheimers type (DAT, n=18).

- Zhang et al. (2010) generalized the Zhang et al. (2009) study with CNE (n=16) and a larger group of patients with DAT (n=46). Patients were separated in three groups (mild, moderate, severe DAT), and each group of patients was contrasted against the CNE.

- Wang et al. (2006) used functional connectivity maps with a seed in the hippocampi to explore the differences between a group of CNE (n=13) and patients with a mild DAT (n=13). All results included in the meta-analysis are from Table 2, seeded in the right hippocampus. Seeds were manually delineated on an individual basis.

- Wang et al. (2007) used functional connectivity maps with a seed in the posterior cingulate cortex (PCC) as well as full brain point-to-point correlations (based on an AAL parcellation) to explore the differences between a group of elderly cognitively normal subjects (CNE, n=14) and patients with a very mild to mild dementia of the Alzheimers type (DAT, n=14). Only the results based on the PCC seed were included in the meta-analysis.

- Goveas et al. (2011) used functional connectivity maps with a seed in the hippocampi to explore the differences between a group of elderly cognitively normal subjects (CNE, n=18) and patients with a mild dementia of

the Alzheimers type (DAT, n=14) before and after donepezil treatment. Seeds were manually delineated on an individual basis, before and after treatment.

- Damoiseaux et al. (2012) used dual-regression independent component analysis to explore longitudinal differences between a group of CNE (n=18) and patients with DAT (n=21). All results included in the meta-analysis are from Table 3 (differences at baseline) and Table 4 (interaction with time). The authors used three components representing the Anterior DMN, Ventral DMN and Posterior DMN.